Springer Theses

# Structured Light Fields

Applications in Optical Trapping, Manipulation, and Organisation

Bearbeitet von
Mike Wördemann

1. Auflage 2012. Buch. xii, 136 S. Hardcover
ISBN 978 3 642 29322 1
Format (B x L): 15,5 x 23,5 cm
Gewicht: 388 g

# Chapter 2
# Introduction to Optical Trapping

Light that is reflected, refracted or absorbed by small particles in general undergoes a change in momentum. In turn, the particles experience an analogous change in momentum, i.e. a resulting force. It was demonstrated already more than 40 years ago that radiation pressure from a (laser) light source can accelerate microscopic particles (Ashkin 1970). The historically most important insight, however, was that microscopic particles cannot only be pushed by the radiation pressure, but they can be at will confined in all three dimensions, leading to the powerful concept of optical tweezers (Ashkin et al. 1986).

This chapter provides a short overview on the basic physical principles and concepts of optical trapping and reviews important milestones. While the focus of this overview will be on classical optical tweezers, related concepts and applications are discussed when beneficial for the understanding of the following chapters.

## 2.1 A Short Note on the History

Although it contradicts everyday experience, it has been accepted ever since the emergence of the electromagnetic theory by Maxwell that light waves are associated with linear momentum (Maxwell 1873). The theoretical treatment consistently substantiates early explanations by Kepler, who believed that the repulsive forces of the sun on comet tails issued from the radiation pressure of the sun light (Lebedev 1901). Even before the invention of lasers, observations with elaborate experimental apparatus proved the existence of radiation pressure qualitatively (Lebedev 1901; Nichols and Hull 1901) and quantitatively (Nichols and Hull 1903). Optical micromanipulation as a means to selectively confine and move small particles, however, requires very high intensity gradients that are only possible with laser light sources. This field of activities was initiated roughly 40 years ago by Ashkin in his seminal paper on "acceleration and trapping of particles by radiation pressure" (Ashkin 1970), who used a weakly focused laser beam in order to guide particles. He not only observed the acceleration of microscopic particles by the radiation force but also noticed a

M. Woerdemann, *Structured Light Fields*, Springer Theses,
DOI: 10.1007/978-3-642-29323-8_2, © Springer-Verlag Berlin Heidelberg 2012

*gradient force*, pulling transparent particles with an index of refraction higher than the surroundings towards the beam axis. Furthermore, he proposed and demonstrated the concept of counter-propagating optical trapping (cf. also Chap. 4), where the opposed radiation pressure of two laser beams leads to the stable three-dimensional confinement of particles. Soon, other stable optical traps were demonstrated, including the optical levitation trap where gravitational forces counteract the radiation pressure (Ashkin and Dziedzic 1971). A major breakthrough in the field of optical micromanipulation was the demonstration of a "single beam gradient force trap", which is nowadays known as *optical tweezers* (Ashkin et al. 1986). In optical tweezers, a single laser beam is very tightly focused through a high numerical aperture lens and by this means can establish gradient forces counteracting the scattering forces in propagation direction. This simple and elegant implementation of an optical trap enables the stable, three-dimensional optical trapping of dielectric particles.

Based on these fundamental findings, a whole field of optical micromanipulation has developed. On the one hand, optical tweezers have been further developed towards versatile, multifunctional tools by means of time-sharing approaches, holographic beam-shaping, and an uncountable number of technological refinements. One the other hand, a wide range of alternative approaches has emerged that go beyond the concept of single or multiple discrete optical tweezers but provide optical landscapes, tailored to a specific problem. A short section at the end of this chapter gives an idea of some of these novel concepts.

## 2.2 Basic Physical Principles of Optical Tweezers

Optical tweezers can be qualitatively understood in terms of geometric ray optics. Consider a spherical, transparent particle in a light field that has an inhomogeneous intensity distribution in a plane transverse to the optical axis, for example a collimated Gaussian beam. Furthermore, we recall that any light ray is associated with linear momentum flux of $p = n_{\mathrm{med}} P/c$, for a ray of power $P$, travelling in a medium with the refractive index $n_{\mathrm{med}}$. Tracing two rays that are incident symmetrically on the sphere but have different intensities, as depicted in Fig. 2.1a, it is easy to see that the vector sum of the momentum flux points away from the region of highest intensity. Consequently, the sphere will experience a reaction force along the intensity gradient, the gradient force $F_{\mathrm{grad}}$ (Ashkin et al. 1986). The gradient force is accompanied by the scattering force $F_{\mathrm{scat}}$ along the optical axis, which is further enhanced by reflection from the surfaces and absorption.

Now consider a tightly focused beam (cf. Fig. 2.1b) as is typical of optical tweezers. The spherical particle acts as a weak positive lens and changes the degree of divergence or convergence of the focused light field. If the angle of the incident rays is high enough, this can result in axial forces $F_{\mathrm{z}}$ that point backward if the particle is positioned behind the focus of the rays. By this means, a stable trapping position for the particle is achieved, i.e. any (small) displacement of the particle will result in a restoring force toward the equilibrium position (Ashkin et al. 1986; Ashkin 1992).

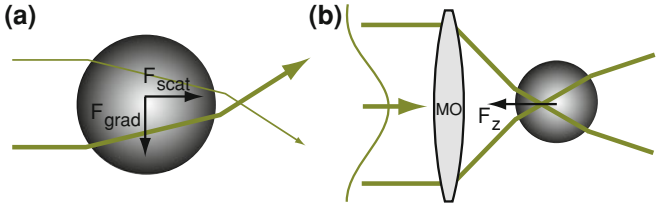


**Fig. 2.1** Basic principle of optical tweezers in the geometric optics regime. **a** A transverse intensity gradient will result in a gradient force $F_{\text{grad}}$ pointing towards the region of highest intensity. **b** Strong focusing through a microscope objective (*MO*) can result in a backward force along the optical axis ($F_z$)

Geometric optics yields a good qualitative picture but can also describe optical tweezers quantitatively if the limits of the regime are respected. Naturally, geometric optics only poorly describes the light field in the vicinity of the focus and furthermore neglects any effects of diffraction and interference (Nieminen et al. 2010; Stilgoe et al. 2008). Hence, geometric optics can only describe the limiting regime of particles that are large compared to the wavelength of the light field ($d \gg \lambda$) (Ashkin 1992). For quantitatively accurate results, as a rule of thumb usually the smallest dimension of the particle should be at least 20 times the optical wavelength (Nieminen et al. 2007).

An alternative approximate description of optical tweezers is the consideration of particles that are very small compared to the wavelength ($d \ll \lambda$). In this *Rayleigh regime*, particles can be seen as infinitesimal induced point dipoles that interact with the light field. It is well known that a sphere of radius $r$ in a homogeneous electric field $\vec{E}$ will be polarised and have an induced dipole moment of (Nieminen et al. 2007)

$$\vec{p}_{\text{dipole}} = 4\pi n_{\text{med}}^2 \epsilon_0 r^3 \left( \frac{m^2 - 1}{m^2 + 2} \right) \vec{E}, \tag{2.1}$$

with the relative refractive index of the particle $m = n_{\text{part}}/n_{\text{med}}$, and the dielectric constant in the vacuum $\epsilon_0$. Owing to this dipole moment, the particle will experience a force in a non-uniform electric field (Harada and Asakura 1996)

$$\vec{F}_{\text{grad}} = \pi n_{\text{med}}^2 \epsilon_0 r^3 \left( \frac{m^2 - 1}{m^2 + 2} \right) \nabla |\vec{E}|^2. \tag{2.2}$$

For small particles, this equation is also valid for a time-varying electric field and in this case, the force can be written in terms of the intensity $I$ of the light field:

$$\vec{F}_{\text{grad}} = \frac{2\pi n_{\text{med}} r^3}{c} \left( \frac{m^2 - 1}{m^2 + 2} \right) \nabla \vec{I}. \tag{2.3}$$

This force obviously depends on the gradient of the intensity and, hence, naturally is called gradient force. It points up the gradient for $m > 1$, i.e. for high-index

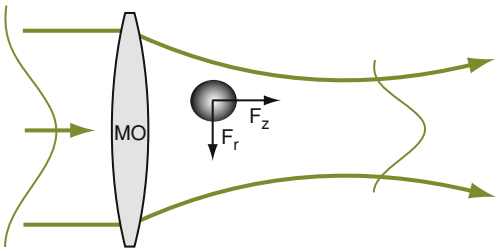


**Fig. 2.2** Basic principle of optical tweezers in the Rayleigh regime. A particle exposed to a light field—a mildly focused Gaussian beam in this example—experiences a transverse force $F_r$ and a force along the beam axis $F_z$

particles. For a static field, this expression would give the total force (Nieminen et al. 2007). In case of time-varying fields, the oscillating dipole can be considered as an antenna that radiates energy. The (vectorial) difference between energy removed from the incident field and energy reradiated by the particle accounts for an associated amount of change in momentum flux and hence results in a scattering force that has a magnitude of (Harada and Asakura 1996)

$$F_{\text{scat}} = \frac{8\pi n_{\text{med}} k^4 r^6}{3c} \left( \frac{m^2 - 1}{m^2 + 2} \right) I, \tag{2.4}$$

with the wavenumber $k = 2\pi/\lambda$. If the particle has absorbing properties, an additional force arises which also depends on the intensity but is proportional to $r^3$ rather than $r^6$ (Nieminen et al. 2010). The sum of these forces, including the gradient force, can be separated into a transverse component $F_r$ and axial component $F_z$ as depicted in Fig. 2.2.

With an increasing degree of focusing, the three-dimensional intensity gradients increase, the (axial) gradient force becomes stronger than the scattering force, and three-dimensional trapping can become possible. Comparing the scaling of the gradient force [Eq. (2.3)] and the scattering force [Eq. (2.4)] with the particle radius, one could expect that small particles below a certain threshold can always be trapped. This is not the case because there is an additional force due to the Brownian molecular motion of the particle. The thermal kinetic energy associated with the Brownian motion is $k_B T$, with the Boltzmann's constant $k_B$ and the temperature $T$. This energy has to be compared to the depth of the optical trapping potential well, generated by the conservative gradient force [1]:

$$U = -\frac{2\pi n_{\text{med}} r^3}{c} \left( \frac{m^2 - 1}{m^2 + 2} \right) I + C, \tag{2.5}$$

where $C$ is an arbitrary integration constant. Furthermore, the drag force due to the dynamic viscosity $\eta$, which is $F_{\text{drag}} = -6\pi\eta r v$ for a spherical particle with radius $r = d/2$ and velocity $v$, will decrease with the radius and thus less efficiently damp the Brownian motion.

[1] The potential energy is derived by integrating Eq. (2.3), assuming that the gradient force is conservative.

Both the geometric optical approximation and the Rayleigh approximation allow for an intuitive understanding of the physical principles of optical trapping, but their quantitative validity is restricted for typically trapped particles, which are often in the order of the optical wavelength ($d \approx \lambda$). In this intermediate regime, a more rigorous treatment based on fundamental electromagnetic theory is required for the quantitatively correct description of optical tweezers.

## 2.3 Optical Trapping as a Scattering Problem

In practice, many particles typically manipulated with optical tweezers, like biological cells or colloidal particles, are in the intermediate regime where the particle size is in the order of the wavelength of the trapping laser light. Furthermore, for optical tweezers the incident light field often is tightly focused to a very small focal spot, in contradiction to the paraxial approximation. Thus, the light fields need to be described rigorously in terms of the full Maxwell equation or the vectorial Helmholtz equation[2] in order to get quantitatively precise results.

In the following we will have a brief look at a rigorous description of optical tweezers that is based on the classical Lorenz-Mie theory and the closely related T-matrix method. In principle, optical trapping of homogeneous, optically linear and isotropic microspheres can be described analytically by Lorenz-Mie solutions (Mie 1908) for the scattering of the incident light at the sphere (Nieminen et al. 2007). The original Lorenz-Mie description, however, is restricted to plane-wave illumination, which obviously is not applicable to optical tweezers. The extension to arbitrary illumination is commonly called *generalised Lorenz-Mie theory* (Gouesbet 2009). Therefore, the incident light field $\vec{E}_{\text{inc}}$ and the scattered light field $\vec{E}_{\text{scat}}$ are represented in terms of vector spherical wavefunctions (VSWFs) (Nieminen et al. 2007):

$$\vec{E}_{\text{inc}} = \sum_{n=1}^{\infty} \sum_{m=-n}^{n} a_{nm} \vec{M}_{nm}^{(3)} + b_{nm} \vec{N}_{nm}^{(3)} \tag{2.6}$$

$$\vec{E}_{\text{scat}} = \sum_{n=1}^{\infty} \sum_{m=-n}^{n} p_{nm} \vec{M}_{nm}^{(1)} + q_{nm} \vec{N}_{nm}^{(1)}. \tag{2.7}$$

Here, $\vec{M}_{nm}^{(i)}$, $\vec{N}_{nm}^{(i)}$ are the VSWFs of the $i$th type, $n$, $m$ are the radial and azimuthal mode indices, and $a_{nm}$, $b_{nm}$, $p_{nm}$, $q_{nm}$ are the expansion coefficients. The choice of VSWFs as the basis for the incident and scattered light field is convenient with respect to the generalised Lorenz-Mie theory (Nieminen et al. 2003). The expansion coefficients usually cannot be found analytically for beams typically used in

[2] We recall that solutions of the Helmholtz equation are solutions of the Maxwell equations if we additionally require that the fields are divergence free, i.e. $\nabla \cdot \vec{E} = 0$ and $\nabla \cdot \vec{H} = 0$ (Novotny and Hecht 2006)

optical tweezers, like the fundamental Gaussian beam or Laguerre-Gaussian beams, but usually are derived numerically because these beams are not exact solutions of the vectorial Helmholtz equation but only solve the paraxial Helmholtz equation (Nieminen et al. 2003). One method is using a least-square fit to produce a representation of the incident light field that matches the (paraxial) beam in the far field (Nieminen et al. 2007; Nieminen et al. 2003). Once the incident light field is given in the representation of Eq. (2.6), the task to solve is finding the $p_{nm}$, $q_{nm}$ of the light field that has been scattered by the particle. When incident and scattered light fields are known, there are straightforward means of calculating the force and torque acting on the particle by considering the (angular) momentum content of the incident and scattered light (Nieminen et al. 2007).

For the case of a homogeneous, isotropic sphere there is no coupling between different modes and, thus, the scattered and incident fields are connected by

$$p_{nm} = a_n a_{nm} \tag{2.8}$$

$$q_{nm} = b_n b_{nm}, \tag{2.9}$$

with the coefficients $a_n$, $b_n$ given by the Lorenz-Mie theory (Nieminen et al. 2007). In the more general case of an arbitrarily shaped particle, coupling needs to be considered and the expansion coefficients of the scattered wave are given by (Nieminen et al. 2007)

$$p_{n'm'} = \sum_{n=1}^{n_{\max}} \sum_{m=-n}^{n} A_{n'm'nm} a_{nm} + B_{n'm'nm} b_{nm} \tag{2.10}$$

$$q_{n'm'} = \sum_{n=1}^{n_{\max}} \sum_{m=-n}^{n} C_{n'm'nm} a_{nm} + D_{n'm'nm} b_{nm}, \tag{2.11}$$

where the infinite sums have been truncated at $n_{\max}$. With the convention that the coefficients $p_{n'm'}$, $q_{n'm'}$ are elements of the column vector $\vec{p}$ and $a_{nm}$, $b_{nm}$ are represented by $\vec{a}$, we can write

$$\vec{p} = \mathbf{T}\vec{a}, \tag{2.12}$$

with the transition matrix $\mathbf{T}$, which often simply is called *T-matrix*. For the case of spherical particles, this matrix is diagonal and completely determined by the Mie coefficients. While the matrix is more complex for a general particle, however, it still only depends on the properties of the particle and is independent of the light field. This particular property is important for the numerical calculation for optical tweezers when the trapping forces or torques at (many) different positions in the light field are of interest or when different light fields are considered. In these cases, the T-matrix only needs to be calculated once for a given particle and can be reused for further calculations, dramatically decreasing calculation times especially for non-spherical particles.

Figure 2.3 shows a few examples of numerical simulations for different numerical apertures of the focusing lens. The numerical code used for these simulations is founded on a publicly available Matlab computational toolbox (Nieminen et al. 2007) and was extended in order to calculate two-dimensional intensity profiles and the full three-dimensional force field. In Fig. 2.3a it can be seen that a Gaussian beam which is focused by a lens with a numerical aperture of NA $= 0.75$ does not create a stable potential well for the particle. Increasing the numerical aperture to NA $= 1.0$ (Fig. 2.3b) yields an equilibrium position for the simulated particle of a diameter of one wavelength and a relative refractive index of $n_{\mathrm{rel}} = n_{\mathrm{part}}/n_{\mathrm{med}} \approx 1.19$. However, this potential minimum is rather shallow and only even stronger focusing (e.g. NA $= 1.34$, Fig. 2.3c) can create a potential well deep enough to trap the particle in the presence of Brownian motion. For all cases it can be seen that the trapping potential is weakest in direction of beam propagation ($+z$) because the scattering force always has a component pointing in this direction which only can be compensated by the gradient force in $-z$ direction.

## 2.4 The Paraxial Approximation

A rigorous treatment of optical tweezers within electromagnetic theory is obviously the favourable approach to obtain a quantitative description of the local forces acting on arbitrary particles. On the other hand, the approximate descriptions derived in Sect. 2.2 proved to be very useful for understanding the physical origin of the optical potential well. In particular, Eq. (2.5) for the optical energy potential due to the gradient force in the Rayleigh regime is valid—assuming the small-particle approximation holds true—for any three-dimensional light intensity distribution $I(\vec{r})$. In the following, we will see that an adequate estimate of the quality of the optical potential landscape can be obtained even when paraxial beams are assumed—an assumption which obviously needs to be carefully discussed in the regime of tightly focused laser beams.

A useful measure for evaluating the validity of the paraxial approximation is the ratio of wavelength $\lambda$ and beam waist $\omega_0$ (Davis 1979)

$$s = \frac{\lambda}{2\pi\omega_0}, \tag{2.13}$$

which should be small for paraxial beams. Tight focusing narrows the beam waist and thus increases the errors introduced by the paraxial approximation. In order to get an impression of the quantity of the errors, we assume a fundamental Gaussian beam which is focused through a microscope objective lens with a numerical aperture of NA $= 1.1$. With the definition of the numerical aperture NA $= n_{\mathrm{med}} \sin(\Theta)$ and the beam waist of $\omega_0 = \lambda/(\pi\Theta)$ (Eichler et al. 2004) and a typical value of the refractive index of the immersion oil $n_{\mathrm{med}} = 1.52$, the parameter $s$ can be

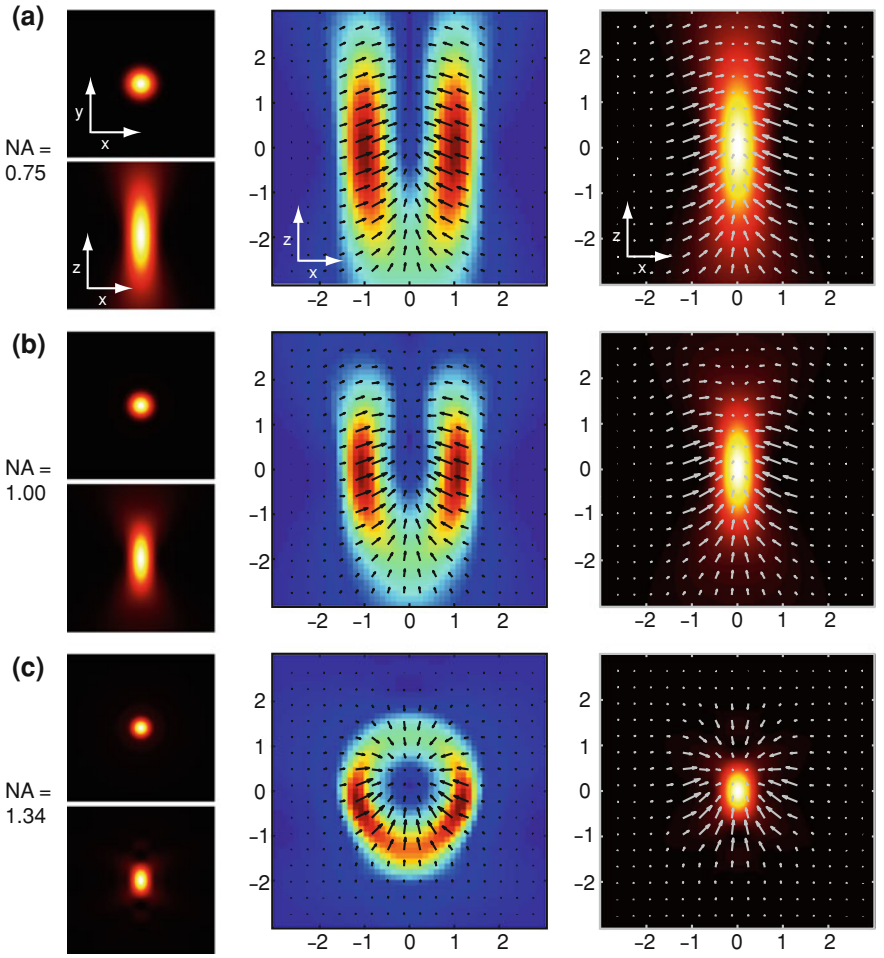


**Fig. 2.3** Optical potential landscape for a spherical particle due to a focused fundamental Gaussian beam propagating in $+z$ direction. Three different numerical apertures for the focusing lens are considered (**a**)–(**c**). In the left column, transverse and longitudinal intensity distributions of the focused light fields are shown. The displayed area is about $3 \times 3$ wavelengths. In the middle column, the numerically calculated local forces acting on the particle are shown (*arrow matrix*). The absolute values are additionally encoded in the colour values behind the *arrow matrix*, emphasising areas of low (*blue*) and high (*red*) forces. In the *right* column, the same force field is displayed upon the intensity distribution, showing the shift between focus position and equilibrium position of the particle. All axes are labelled in units of wavelength. The particle is assumed to have a diameter of one wavelength and a refractive index of $n_{\text{particle}} = 1.59$; the surrounding fluid is assumed to have a refractive index of $n_{\text{med}} = 1.34$ (water)

calculated as[3] $s \approx 0.4$. For this regime, following Barton and Alexander (Barton and Alexander 1989), an average deviation of the electric field of approximately 20% from the rigorous treatment can be expected. Although this is a large error, and the maximal error can be even more significant in particular locations in the vicnity of the focus, it can be expected that the qualitative structure of the field is adequately described. In order to increase the accuracy, higher order terms can be included. For the same value $s \approx 0.4$, a fifth order approximation yields an average error of only approximately 3%.

## 2.5 Measuring Forces

One of the unique features of optical tweezers is their ability not only to transfer extremely small forces to micro- and nanoscopic particles but also to measure forces in the piconewton range with high precision. Although, in principle, the optical potential is known from the intensity distribution in the sample [cf. Eq. (2.5)] (Viana et al. 2007), the usual way is to probe the potential with a particle of the same kind as is to be used for the force measurement. This automatically eliminates a couple of experimental uncertainties, such as transmission properties of the microscope objective, the exact transverse beam profile, or effects due to the small-particle approximation, and includes them in the calibration. For the calibration, a particle is trapped in the optical potential well and its motion due to the Brownian molecular motion is monitored. As illustrated in Fig. 2.4a, the particle automatically scans or "explores" the shape of the potential well, having a higher probability of presence at the minimum of the potential well. Figure 2.4b shows the number $N(x)$ that a particle was observed at a particular position $x$, which gives the probability function $p(x)$. Often, an optical potential induced by optical tweezers can be approximated as harmonic (cf. Fig. 2.4c). In that case the calibration procedure yields a scalar calibration factor $k$, the stiffness of the optical trap. In this approximation, the force a particle feels is directly proportional to its displacement $\Delta x$ from the equilibrium position ($x = 0$), i.e. $|\vec{F}| = k\Delta x$. Force measurement in this configuration means measuring the new equilibrium position and thus $\Delta x$ as illustrated in Fig. 2.4d. As the displaced particle still underlies Brownian motion, the measured force always is a superposition of external forces and forces due to Brownian motion. The uncertainty due to Brownian motions decreases with measurement time as the mean value of the stochastic process is exactly the (displaced) equilibrium position.

[3] Note that the $s$ parameter is independent of the wavelength.

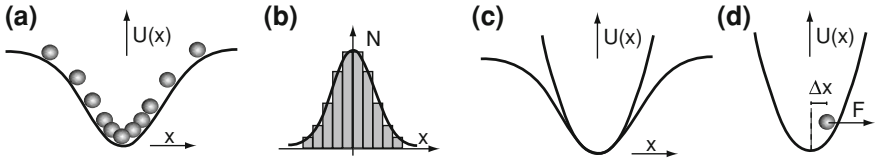


**Fig. 2.4** Basic principles of force measurement. A trapped particle has a higher probability of presence at the potential minimum (**a**), resulting in an according histogram of positions (**b**). For typical configurations and applications, the potential well can be approximated as harmonic (**c**), resulting in a linear relation between external forces acting on the particle and the particle's displacement (**d**)

### *2.5.1 Particle Position Detection*

All methods for the calibration of optical trapping potentials rely on the position tracking of a probe particle. Two methods have established for particle tracking in optical tweezers. The (lateral) particle position can be detected by observing the laser light transmitted through the particle or reflected from it. The interference pattern, e.g. of the transmitted light and the light not influenced by the particle, is detected, usually in the back focal plane of the condenser, by means of a position sensitive semiconductive sensor (Tolić-Nørrelykke et al. 2006). The sensor can be a lateral effect detector or, more frequently used, a quadrant photo diode. Tracking the intensity maximum in the back focal plane enables highly sensitive position detection of the particle. The total intensity, summed over all four quadrants of the photo diode, also gives a convenient measure of the axial position of the particle (Ghislain et al. 1994). Instead of the trapping laser, an additional laser can be used to detect the particle position.

As an alternative to photo diode based position detection, video microscopy with subsequent image analysis has gained importance with the advent of high resolution, high-speed digital video cameras in recent years (Gibson et al. 2008). While position detection with video microscopy is very flexible—e.g. it can easily be extended to multiple traps—the precision in position detection usually is lower compared to laser tracking schemes, owing to the relatively large pixel size of a typical video camera sensor. Also, the temporal resolution of video based position detection is still at least an order of magnitude lower than direct tracking of the laser beam, even with high-end video cameras.

### *2.5.2 Calibration Schemes*

Having the position data of a trapped particle, there are several ways to characterise and calibrate the optical potential well and deduce the trap stiffness $k$ (Neuman and Block 2004). For a harmonic potential, the overdamped oscillation of a particle in the optical trap can be described analytically and the power spectrum of the dynamics

can be written as a Lorentzian distribution (Svoboda and Block 1994):

$$S(f) = \frac{k_B T}{2\pi^3 \beta \left(f_0^2 + f^2\right)}. \tag{2.14}$$

Here, $\beta$ is the viscous drag coefficient of the particle and $f_0 = k/(2\pi\beta)$ the corner frequency which can be deduced from a best fit to the power spectrum with Eq. (2.14). For a free sphere with radius $r$ far away from any surface, the viscous drag coefficient is known to be $\beta = 6\pi\eta r$ while it has to be corrected in the vicinity of a surface by a distance-dependent factor given by Faxen's law (Svoboda and Block 1994). With a known viscous drag and the corner frequency determined from the power spectrum, the trap stiffness can be calculated. Precise calibration requires to consider further influences on the power spectrum, including frequency dependence of the drag force, effects due to the finite sampling frequency or frequency dependence of the position detection sensor (Berg-Sørensen and Flyvbjerg 2004).

The trap stiffness can also be determined by monitoring the variance of the thermal fluctuation of a trapped particle. The equipartition theorem gives the thermal kinetic energy of a particle which can be related to the optical potential energy of a trap with stiffness $k$ (Neuman and Block 2004):

$$\frac{1}{2} k_B T = \frac{1}{2} k < x^2 >, \tag{2.15}$$

where $< x^2 >$ is the variance of the displacement from the equilibrium position. While the simplicity of this method, in particular the independence from the viscosity of the medium, is a clear advantage, it is hard to detect errors because the variance is an "intrinsically biased estimator" (Neuman and Block 2004). Since variance is derived from the square of a quantity, any noise or drift will always increase the variance and leads to an apparent decrease of the determined stiffness.

From the optical potential well, however, the probability function for the displacement of a trapped particle can be deduced (Florin et al. 1998):

$$p(x) = \exp\left(\frac{-U(x)}{k_B T}\right) = \exp\left(\frac{-kx^2}{2k_B T}\right), \tag{2.16}$$

where the first equals sign is valid for any potential $U(x)$ while the second sign holds true only for a harmonic potential.

Alternatively, the optical potential can also be probed by applying known forces and monitoring the displacement for different forces (Felgner et al. 1995). The applied force usually is viscous drag force on the particle. Consequently, all considerations on the drag force discussed above are valid. In principle it is possible to apply a discrete number of different forces or rather choose a continuous function like a sinusoidally varying force. As with the probability function, the drag force method is suitable to characterise even non-harmonic potentials. Furthermore, this method gives a straightforward way to determine the maximal force or the depth of the

potential well by increasing the applied force until the particle escapes from the optical trap (Neuman and Block 2004; Malagnino et al. 2002).

In typical biological samples often particular local parameters are not directly accessible. For example, it might be difficult to determine the viscosity of the medium surrounding a trapped organelle or reference bead inside a biological cell. Furthermore, the local temperature usually is unknown as the laser focus of the optical trap induces thermal energy and heats up the sample depending on the absorption properties. A combination of the calibration schemes discussed above, however, can yield enough independent parameters to enable real-time in situ calibration even in complex biological systems (Wan et al. 2009).

## 2.6 Dynamic Optical Tweezers

Although single optical tweezers at a fixed position already enable many applications, it is often desirable to have a trap that can be displaced in the sample chamber. In Fig. 2.5a the basic configuration of optical tweezers is depicted. A collimated laser beam is focused through a lens with short focal length, which usually is a microscope objective, into a sample chamber that contains a fluid with dispersed particles. In order to move the focal spot and thus the optical trap to a different position in the plane orthogonal to the beam axis, the incident laser beam needs to have an angle with respect to the beam axis as shown in Fig. 2.5b. A diverging or converging beam, on the other hand, would shift the focal plane along the beam axis (Fig. 2.5c).

It is important that the beam hits the back aperture of the microscope objective always with the same diameter and at the same, centred position in order to keep the optical trap operating and its properties unchanged (Ashkin 1992; Fällman and Axner 1997). One possibility is to use an afocal telescope of two lenses in order to create an optically conjugated plane of the back aperture of the microscope objective (cf. Fig. 2.5d). Any angle introduced at this plane, e.g. by a gimbal mounted mirror (Fällman and Axner 1997), will result in a corresponding angle at the back aperture of the microscope objective without a shift in position. Similarly, any divergence introduced with a constant beam diameter at this plane, will be reproduced with a constant beam diameter at the back aperture of the microscope objective.

Position control can be automated if computer-controlled scanning mirrors are used (Sasaki et al. 1991; Misawa et al. 1992; Visscher et al. 1993). A similar approach uses acousto-optic deflectors (AODs) at the conjugate plane (Simmons et al. 1996). AODs can introduce an angle by utilising a dynamic Bragg grating inside a piezoelectric material and this function principle allows for an extremely high rate of different deflection angles to be set. One powerful application is time-shared optical tweezers, where the laser beam is directed to one position, held there for a short time and then directed to the next position. If this is done iteratively and the stopover at each position is long enough to pull back a particle to the centre position, and also the absence of the laser beam is short enough to prevent the particles escaping due

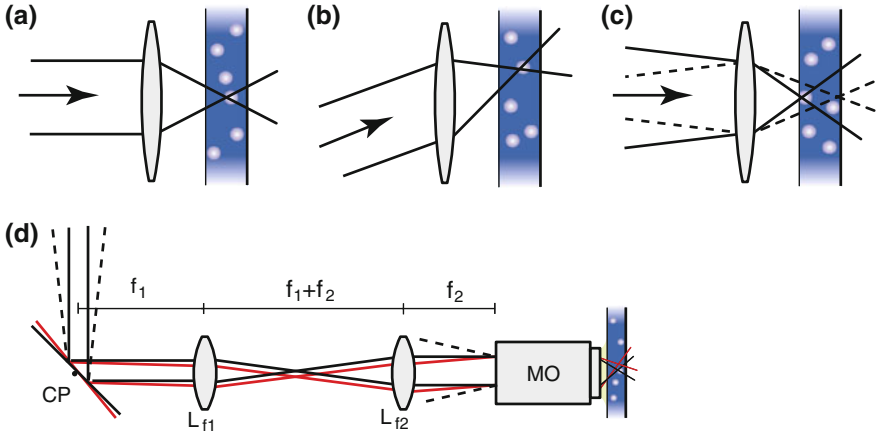


**Fig. 2.5** Basic principle of position control in optical tweezers. **a–c** The position of the laser focus and hence the optical trap is translated three-dimensionally by variation of the incidence angle and divergence of the laser beam. **d** Technical realisation with a Keplarian telescope ($L_{f1}$, $L_{f2}$) and beam manipulation in a conjugate plane (*CP*) of the back aperture of a microscope objective (MO). From (Woerdemann et al. 2012)

to Brownian motion, many particles can be trapped quasi simultaneously (Sasaki et al. 1991; Visscher et al. 1993; Mio et al. 2000; Mirsaidov et al. 2008).

One ingenious way to realise control of beam angle and beam divergence in one particular plane without mechanical manipulation is diffraction at computer-generated holograms, also known as *diffractive optical elements* (DOEs) in this context. The hologram can be imprinted statically in optical materials (Dufresne and Grier 1998; Dufresne et al. 2001), e.g. by lithographic methods, or alternatively displayed by a computer-controlled spatial light modulator (SLM) (Reicherter et al. 1999; Liesener et al. 2000). The latter implementation enables versatile spatio-temporal structuring of the light field, leading to dynamic holographic optical tweezers (HOT) (Curtis et al. 2002). The classical use of HOT is the generation of multiple optical traps simultaneously. A thorough discussion of the fundamental concepts of HOT will be provided in Chap. 7.

## 2.7 Some Applications of Single Optical Tweezers

Optical tweezers have found a huge number of applications since their first demonstration by Arthur Ashkin and colleagues 25 years ago (Ashkin et al. 1986). In particular biological questions on a single cell or single-molecule (Svoboda and Block 1994; Stevenson et al. 2010) level can be well addressed with optical tweezers for two reasons. First, there is no other tool available that enables handling of single cells, organelles, and macromolecules with such a flexibility and precision at the

same time without any physical contact that could possibly contaminate a sample. Second, optical tweezers can be used to exert defined forces and, more importantly, measure extremely small forces with an unrivalled precision (Neuman and Block 2004; Berg-Sørensen and Flyvbjerg 2004; Florin et al. 1998; Ghislain and Webb 1993; Jahnel et al. 2011).

Further applications of optical tweezers and closely related methods can be found in such diverse fields as colloidal sciences (Grier 1997), microfluidics (Leach 2006; MacDonald et al. 2003), microscopic alignment (Friese et al. 1998; O'Neil and Padgett 2002), particle separation (Imasaka et al. 1995) and sorting (MacDonald et al. 2003; Perch-Nielsen et al. 2009; Jonas and Zemanek 2008), or molecular motor dynamics (Asbury et al. 2003; Maier 2005). Optical tweezers experiments can answer fundamental physical questions, including the direct transfer of optical angular momentum (O'Neil et al. 2002; He et al. 1995), hydrodynamic interactions (Meiners and Quake 1999; Crocker 1997), and—of course—light-matter interaction (Dholakia and Zemanek 2010).

It has been demonstrated that dynamically steered and modulated optical tweezers can generate an optical thermal ratchet that biases the Brownian motion of diffusing particles (Faucheux et al. 1995). Quite recently, highly interesting insights into the physical origins of Brownian motion at very short time scales were obtained, where random diffusion is originated by ballistic motion processes (Huang et al. 2011).

This list is by no means exhaustive or complete but represents a small selection of interesting applications; an excellent overview can be found, for example, in Reference (Padgett et al. 2010).

## 2.8 Optical Angular Momentum and Torque

Of particular interest from the fundamental physical point of view is the ability of light fields not only to transfer linear momentum to matter but also *spin angular momentum* (SAM) and *orbital angular momentum* (OAM). SAM is strongly related to the polarisation state of light, resulting in a value of $|\vec{S}| = \pm\hbar$ per photon for circularly polarised light, where the sign is given by the chirality. An experimental proof of this relation was shown in the famous experiment by Beth (Beth 1936).

OAM is related to a tilt of the wavefront. In case of a screw wavefront dislocation with $\exp(i\ell\varphi)$ azimuthal phase dependence, also called an optical vortex, the pitch of the screw defines the topological charge $\ell$. The orbital angular momentum then is given as $\ell\hbar$ per photon (Allen et al. 1992; Leach et al. 2002). A direct experimental validation of this relation was done with optical tweezers only quite recently (He et al. 1995) compared to the experimental proof of spin angular momentum.

SAM and OAM decouple in the paraxial approximation (Berry 1998; Barnett 2002) but may be transferred into each other in strongly focused beams (Nieminen et al. 2008). While spin angular momentum always is intrinsic in the sense that its value does not depend on the choice of calculation axis, OAM may be either intrinsic or extrinsic (O'Neil et al. 2002).

Low-order Laguerre-Gaussian (LG) beams are the experimentally most easily realised light fields with orbital angular momentum. Mathematically, LG beams are a complete set of free-space solutions (Okulov 2008; Saleh and Teich 2008) of the paraxial wave equation in the cylindrical system of coordinates (Saleh and Teich 2008; Dholakia and Lee 2008):

$$\mathrm{LG}_p^\ell(\vec{r}) \propto \left(\frac{r}{\omega(z)}\right)^\ell \mathrm{L}_p^\ell\left(\frac{2r^2}{\omega^2(z)}\right) \exp\left[\left(\frac{-r^2}{\omega^2(z)}\right) + i\left(\frac{-kr^2}{2R(z)} + (2p+\ell+1)\Phi_G(z) - \ell\varphi\right)\right]. \tag{2.17}$$

Here, $z, r, \varphi$ are coordinates in the cylindrical system of coordinates, $\mathrm{L}_p^\ell$ are the generalised Laguerre polynomials, $p, \ell$ are mode parameters and $\ell$ also determines the topological charge, $\omega(z)$ indicates the diameter of the beam, $R(z)$ the phase front curvature, and $\Phi_G(z)$ the Gouy phase shift.[4]

LG beams are self-similar in a sense that they maintain their transverse intensity profile during propagation except for a radial scaling factor. Of particular importance for optical trapping applications are modes with $p = 0$, which have the shape of a single ring or "doughnut". Particles are confined to this ring by transverse gradient forces and feel torque due to a transfer of OAM. In consequence, particles can move continuously on the ring of high intensity.

### 2.8.1 Generation of Light Fields Carrying Orbital Angular Momentum

LG beams can be generated in various ways, usually by converting other laser modes like the fundamental Gaussian $\mathrm{TEM}_{00}$ mode or higher modes. The *astigmatic mode converter* that consists of two cylindrical lenses with suitable distance utilises the property that any LG and Hermite-Gaussian (HG) mode can be composed of a finite number of HG modes (Allen et al. 1992; Beijersbergen et al. 1993).[5] With appropriate choice of the transverse input angle, an incident (higher order) HG mode can be decomposed in different HG modes that gain a different (Gouy) phase shift while being transmitted through the cylindrical lenses. The input HG mode and the relative phase shift between the decomposed modes can be chosen in a way that the output is a desired LG mode. The conversion efficiency of this mode converter is rather high and the mode purity can be high but it is very sensitive to the alignment and also the requirement for specific higher order HG modes is a limitation (Beijersbergen et al. 1993).

Mode conversion from a fundamental Gaussian ($\mathrm{TEM}_{00}$) beam, which is readily available in high quality from the majority of commercial lasers, into an LG beam

[4] To keep the presentation concise, some quantities are only loosely defined here. Cf. Chap. 6, Sect. 6.1 for a more rigorous definition.

[5] More strictly speaking, LG as well as HG modes are a complete, orthogonal basis of solutions of the paraxial wave equation. Thus, any HG or LG mode can be expanded in a finite series of either modes (Beijersbergen et al. 1993).

can be achieved by imprinting the vortex phase term $\exp(i\ell\varphi)$ explicitly onto the Gaussian beam by means of a spiral phase plate (Beijersbergen et al. 1994). Depending on the overlap of input mode and desired output mode, this approach couples a majority of the input power into a desired $\mathrm{LG}^{\ell}_{p=0}$ output mode. However, still a significant part usually couples into higher $p$-modes, resulting in higher order rings besides the desired doughnut shape (Ando et al. 2009). The output mode purity can be significantly increased if the input beam is pre-shaped to resemble the shape of the doughnut beam before passing the spiral phase plate (Machavariani et al. 2002).

A mode converter that has not yet found wide application but is interesting from the fundamental point of view can be realised with second-harmonic generation (SHG). An LG beam that undergoes SHG results in another LG beam that does not only possess twice the frequency, but also doubles the index $\ell$ of the mode (Dholakia et al. 1996). By this means, higher order $\ell$ modes can be derived from lower order LG modes.

A very versatile approach to generate arbitrary LG modes is the use of computer-generated holograms (CGHs). In the simplest case these CGHs can be seen as a diffractive, usually off-axis, equivalent of a spiral phase plate that enables the generation of any arbitrary $\mathrm{LG}^{\ell}_{p=0}$ mode (Heckenberg et al. 1992) or $LG^{\ell=0}_{p}$ mode (Arlt et al. 1998). CGHs can be tailored for optimal efficiency or optimal purity of the produced output *LG* modes (Arlt et al. 1998) with remarkable results. In particular with computer-addressable SLMs, holographic mode conversion can be performed in a very flexible way. By this means, even much complexer beams that also carry OAM can be created, like higher order Bessel beams (Volke-Sepulveda et al. 2002) or helical Mathieu beams (Chavez-Cerda et al. 2002). The holographic generation of complex beams, although not with an emphasis on orbital angular momentum, will be comprehensively discussed in Chap. 5 on non-diffracting Mathieu beams and Chap. 6 on self-similar Ince-Gaussian beams. Complex superpositions of different light beams carrying OAM enable tailoring local OAM density and intensity, leading to possibly highly exciting optical landscapes (Zambrini and Barnett 2007).

### 2.8.2 *Measurement and Applications of Optical Angular Momentum*

The standard method for detecting the OAM content of a light field is to create an interferogram between the field under investigation and a reference field, usually a plane wave or $\mathrm{TEM}_{00}$ mode or a higher LG or HG mode (Padgett et al. 1995). The detection of the full OAM content of a arbitrary light field, however, is a non-trivial task and methods have been proposed and used to solve it under certain constraints (Parkin et al. 2006). The total SAM of a light field on the other hand is relatively easy to access by measuring the polarisation state of the light field (Parkin et al. 2006). By dynamic application of (known) SAM states, the total optical angular momentum and thus the OAM can be derived (Parkin et al. 2006; Simpson et al. 1997).

Optical angular momentum can be transferred to matter by various physical principles (Padgett and Bowman 2011). Absorption is a universal means to transfer SAM as well as OAM, i.e. absorbed photons transfer their SAM and OAM to the particle that absorbs the light. If the light is not (completely) absorbed, the difference between incident and scattered light gives the amount of transferred optical angular momentum. The SAM content of a light wave can be altered by birefringent properties of a particle. If a particle, for example, transforms (a portion of) linearly polarised incident light into circularly polarised light, the SAM of the light wave increases by $\hbar$ per photon and the particle feels the opposite amount of angular momentum in order to conserve the total amount of angular momentum. OAM an the other hand can be transferred if a particle changes the wave front tilt of the incident light wave. A microscopic version of a spiral phase plate, for example, transfers light without OAM into light carrying OAM (Asavei et al. 2009). The negative difference is transferred to the particle.

Probably the most exciting field of applications of optical angular momentum in the field of micromanipulation is the continuous driving of micro machines (Padgett and Bowman 2011; Asavei et al. 2009; Ladavac and Grier 2004). Light waves carrying optical angular momentum are also utilised in quantum optics where, e.g. the transfer of information encoded in OAM states of light (Gibson et al. 2004) is of current interest. A review of recent developments in this area can be found elsewhere (Franke-Arnold et al. 2008).

## 2.9 Conclusion and Perspectives

The basic concept of optical trapping has developed into many branches that partly share only the basic physical process of (angular) momentum transfer from light to matter with the original optical tweezers. In particular the sophisticated shaping of light fields has attracted many researchers in recent years and a multitude of exciting applications have arisen. The most prominent application scenario probably is the flexible creation of multiple individual spots. In Chap. 7 we will discuss holographic optical tweezers which are versatile tools enabling the dynamic generation of hundreds of individual traps simultaneously. With "generalised phase contrast", a competing technique for the generation of multiple traps has emerged (Glückstad and Palima 2009). In Chap. 3, a more advanced phase contrast method, holographic phase contrast, is introduced. A couple of higher order light modes have also been proposed and partly demonstrated for exciting applications in optical micromanipulation. In Chap. 5, for example, we will see that non-diffracting beams have many desirable features making them a promising choice for the creation of three-dimensionally structured matter. Higher order Gaussian beams and in particular the class of Ince-Gaussian beams discussed in Chap. 6 can significantly aid in applications like the organisation of microparticles, where a high degree of order is aimed at. A holographically generated array of $\mathrm{LG}_{p=0}^{\ell}$ beams was shown to be capable of creating and driving microscopic pumps that can generate a micro flow in

situ (Ladavac and Grier 2004). Quite recently, it has been demonstrated that absorbing particles can be trapped in air, utilising tube-shaped (Desyatnikov et al. 2009; Shvedov et al. 2009; Shvedov et al. 2010) and bottle-shaped hollow light fields (Shvedov et al. 2010; Zhang and Chen 2011) and employing photophoretic forces (Kerker and Cooke 1982) rather than optical forces. Again, as with the examples of applications of single optical tweezers, the list of exciting innovations is endless and the mentioned works are only an arbitrary selection. Many more examples, however, will be provided within the following chapters.

## References

Allen L, Beijersbergen M, Spreeuw R, Woerdman J (1992) Orbital angular momentum of light and the transformation of laguerre-gaussian laser modes. Phys Rev A 45:8185–8189

Ando T, Ohtake Y, Matsumoto N, Inoue T, Fukuchi N (2009) Mode purities of Laguerre-Gaussian beams generated via complex-amplitude modulation using phase-only spatial light modulators. Opt Lett 34:34–36

Arlt J, Dholakia K, Allen L, Padgett M (1998) The production of multiringed Laguerre-Gaussian modes by computer-generated holograms. J Mod Opt 45:1231–1237

Asavei T, Nieminen T, Heckenberg N, Rubinsztein-Dunlop H (2009) Fabrication of microstructures for optically driven micromachines using two-photon photopolymerization of UV curing resins. J Opt A: Pure Appl Opt 11:034001

Asbury C, Fehr A, Block S (2003) Kinesin moves by an asymmetric hand-over-hand mechanism. Science 302:2130–2134

Ashkin A (1970) Acceleration and trapping of particles by radiation pressure. Phys Rev Lett 24:156–159

Ashkin A (1992) Forces of a single-beam gradient laser trap on a dielectric sphere in the ray optics regime. Biophys J 61:569–582

Ashkin A, Dziedzic J (1971) Optical levitation by radiation pressure. Appl Phys Lett 19:283

Ashkin A, Dziedzic J, Bjorkholm J, Chu S (1986) Observation of a single-beam gradient force optical trap for dielectric particles. Opt Lett 11:288–290

Barnett S (2002) Optical angular-momentum flux. J Opt B: Quantum Semiclass Opt 4:S7

Barton J, Alexander D (1989) 5th-Order corrected electromagnetic-field components for a fundamental Gaussian beam. J Appl Phys 66:2800–2802

Beijersbergen M, Allen L, van der Veen H, Woerdman J (1993) Astigmatic laser mode converters and transfer of orbital angular momentum. Opt Commun 96:123–132

Beijersbergen M, Coerwinkel R, Kristensen M, Woerdman J (1994) Helical-wave-front laser-beams produced with a spiral phaseplate. Opt Commun 112:321–327

Berg-Sørensen K, Flyvbjerg H (2004) Power spectrum analysis for optical tweezers. Rev Sci Instrum 75:594–612

Berry M (1998) Paraxial beams of spinning light. In: Soskin M (ed) International conference on singular optics, vol 3487. SPIE Proceedings pp 6–11

Beth R (1936) Mechanical detection and measurement of the angular momentum of light. Phys Rev 50:115–125

Chavez-Cerda S, Padgett M, Allison I, New G, Gutierrez-Vega J, O'Neil A, MacVicar I, Courtial J (2002) Holographic generation and orbital angular momentum of high-order Mathieu beams. J Opt B: Quantum Semiclass Opt 4:S52–S57

Crocker J (1997) Measurement of the hydrodynamic corrections to the Brownian motion of two colloidal spheres. J Chem Phys 106:2837–2840

Curtis J, Koss B, Grier D (2002) Dynamic holographic optical tweezers. Opt Commun 207:169–175
Davis L (1979) Theory of electromagnetic beams. Phys Rev A 19:1177–1179
Desyatnikov A, Shvedov V, Rode A, Krolikowski W, Kivshar Y (2009) Photophoretic manipulation of absorbing aerosol particles with vortex beams: theory versus experiment. Opt Express 17:8201–8211
Dholakia K, Lee W (2008) Optical trapping takes shape: the use of structured light fields. Adv Atom Mol Opt Phys 56:261–337
Dholakia K, Zemanek P (2010) Colloquium: gripped by light: optical binding. Rev Mod Phys 82:1767
Dholakia K, Simpson N, Padgett M, Allen L (1996) Second-harmonic generation and the orbital angular momentum of light. Phys Rev A 54:R3742–R3745
Dufresne E, Grier D (1998) Optical tweezer arrays and optical substrates created with diffractive optics. Rev Sci Instrum 69:1974–1977
Dufresne E, Spalding G, Dearing M, Sheets S, Grier D (2001) Computer-generated holographic optical tweezer arrays. Rev Sci Instrum 72:1810–1816
Eichler J, Dünkel L, Eppich B (2004) Die Strahlqualität von Lasern: Wie bestimmt man Beugungsmaßzahl und Strahldurchmesser in der Praxis?
Fällman E, Axner O (1997) Design for fully steerable dual-trap optical tweezers. Appl Opt 36:2107–2113
Faucheux L, Bourdieu L, Kaplan P, Libchaber A (1995) Optical thermal ratchet. Phys Rev Lett 74:1504–1507
Felgner H, Muller O, Schliwa M (1995) Calibration of light forces in optical tweezers. Appl Opt 34:977–982
Florin E, Pralle A, Stelzer E, Horber J (1998) Photonic force microscope calibration by thermal noise analysis. Appl Phys A 66:S75–S78
Franke-Arnold S, Allen L, Padgett M (2008) Advances in optical angular momentum. Laser Photon Rev 2:299–313
Friese M, Nieminen T, Heckenberg N, Rubinsztein-Dunlop H (1998) Optical alignment and spinning of laser-trapped microscopic particles. Nature 394:348–350
Ghislain L, Webb W (1993) Scanning-force microscope based on an optical trap. Opt Lett 18:1678–1680
Ghislain L, Switz N, Webb W (1994) Measurement of small forces using an optical trap. Rev Sci Instrum 65:2762–2768
Gibson G, Courtial J, Padgett M, Vasnetsov M, Pas'ko V, Barnett S, Franke-Arnold S (2004) Free-space information transfer using light beams carrying orbital angular momentum. Opt Express, 12:5448–5456
Gibson G, Leach J, Keen S, Wright A, Padgett M (2008) Measuring the accuracy of particle position and force in optical tweezers using high-speed video microscopy. Opt Express 16:14561–14570
Glückstad J, Palima D (2009) Generalized Phase Contrast: Applications in Optics and Photonics. Springer, Netherlands
Gouesbet G (2009) Generalized Lorenz-Mie theories, the third decade: a perspective. J Quant Spectrosc Ra 110:1223–1238
Grier D (1997) Optical tweezers in colloid and interface science. Curr Opin Colloid In 2:264–270
Harada Y, Asakura T (1996) Radiation forces on a dielectric sphere in the Rayleigh scattering regime. Opt Commun 124:529–541
He H, Friese M, Heckenberg N, Rubinsztein-Dunlop H (1995) Direct observation of transfer of angular momentum to absorptive particles from a laser beam with a phase singularity. Phys Rev Lett 75:826–829
Heckenberg N, McDuff R, Smith C, White A (1992) Generation of optical phase singularities by computer-generated holograms. Opt Lett 17:221–223

Huang R, Chavez I, Taute K, Lukic B, Jeney S, Raizen M, Florin E (2011) Direct observation of the full transition from ballistic to diffusive brownian motion in a liquid. Nat Phys 7:576–580
Imasaka T, Kawabata Y, Kaneta T, Ishidzu Y (1995) Optical chromatography. Anal Chem 67:1763–1765
Jahnel M, Behrndt M, Jannasch A, Schäffer E, Grill S (2011) Measuring the complete force field of an optical trap. Opt Lett 36:1260–1262
Jonas A, Zemanek P (2008) Light at work: the use of optical forces for particle manipulation, sorting, and analysis. Electrophoresis 29:4813–4851
Kerker M, Cooke D (1982) Photophoretic force on aerosol-particles in the free-molecule regime. J Opt Soc Am 72:1267–1272
Ladavac K, Grier D (2004) Microoptomechanical pumps assembled and driven by holographic optical vortex arrays. Opt Express 12:1144–1149
Leach J (2006) An optically driven pump for microfluidics. Lab Chip 6:735–739
Leach J, Padgett M, Barnett S, Franke-Arnold S, Courtial J (2002) Measuring the orbital angular momentum of a single photon. Phys Rev Lett 88:257901
Lebedev P (1901) Untersuchungen über die Druckkräfte des Lichtes. Ann Phys 6:433
Liesener J, Reicherter M, Haist T, Tiziani H (2000) Multi-functional optical tweezers using computer-generated holograms. Opt Commun 185:77–82
MacDonald M, Spalding G, Dholakia K (2003) Microfluidic sorting in an optical lattice. Nature, 426:421–424
Machavariani G, Davidson N, Hasman E, Blit S, Ishaaya A, Friesem A (2002) Efficient conversion of a Gaussian beam to a high purity helical beam. Opt Commun 209:265–271
Maier B (2005) Using laser tweezers to measure twitching motility in neisseria. Curr Opin Microbiol 8:344–349
Malagnino N, Pesce G, Sasso A, Arimondo E (2002) Measurements of trapping efficiency and stiffness in optical tweezers. Opt Commun 214:15–24
Maxwell J (1873) A treatise on electricity and magnetism. vol 2, Clarendon Press, Oxford
Meiners J, Quake S (1999) Direct measurement of hydrodynamic cross correlations between two particles in an external potential. Phys Rev Lett 82:2211–2214
Mie G (1908) Beiträge zur Optik trüber Medien, speziell kolloidaler Metallösungen. Ann Phys 25:377–445
Mio C, Gong T, Terray A, Marr D (2000) Design of a scanning laser optical trap for multiparticle manipulation. Rev Sci Instrum 71:2196–2200
Mirsaidov U, Scrimgeour J, Timp W, Beck K, Mir M, Matsudaira P, Timp G (2008) Live cell lithography: using optical tweezers to create synthetic tissue. Lab Chip 8:2174–2181
Misawa H, Sasaki K, Koshioka M, Kitamura N, Masuhara H (1992) Multibeam laser manipulation and fixation of microparticles. Appl Phys Lett 60:310–312
Neuman K, Block S (2004) Optical trapping. Rev Sci Instrum 75:2787–2809
Nichols E, Hull G (1901) A preliminary communication on the pressure of heat and light radiation. Phys Rev (Series I) 13:307–320
Nichols E, Hull G (1903) The pressure due to radiation (second paper). Phys Rev (Series I) 17:26–50
Nieminen T, Rubinsztein-Dunlop H, Heckenberg N (2003) Multipole expansion of strongly focussed laser beams. J Quant Spectrosc Ra 79:1005–1017
Nieminen T, Knoner G, Heckenberg N, Rubinsztein-Dunlop H (2007) Physics of optical tweezers. Laser Manipulation Cells Tissues 82:207–236
Nieminen T, Loke V, Stilgoe A, Knoner G, Branczyk A, Heckenberg N, Rubinsztein-Dunlop H (2007) Optical tweezers computational toolbox. J Opt A: Pure Appl Opt 9:S196–S203
Nieminen T, Stilgoe A, Heckenberg N, Rubinsztein-Dunlop H (2008) Angular momentum of a strongly focused gaussian beam. J Opt A: Pure Appl Opt 10:115005
Nieminen T, Stilgoe A, Heckenberg N, Rubinsztein-Dunlop H (2010) Approximate and exact modeling of optical trapping. SPIE Proc 7762:77622V
Novotny L, Hecht B (2006) Principles of nano-optics. Cambridge University Press, Cambridge

Okulov A (2008) Angular momentum of photons and phase conjugation. J Phys B: At Mol Opt Phys 41:101001
O'Neil A, Padgett M (2002) Rotational control within optical tweezers by use of a rotating aperture. Opt Lett 27:743–745
O'Neil AT, MacVicar I, Allen L, Padgett MJ (2002) Intrinsic and extrinsic nature of the orbital angular momentum of a light beam. Phys Rev Lett 88:053601
Padgett M, Bowman R (2011) Tweezers with a twist. Nat Photonics 5:343–348
Padgett M, Arlt J, Simpson N, Allen L (1995) An experiment to observe the intensity and phase structure of Laguerre-Gaussian laser modes. Am J Phys 64:77–82
Padgett M, Molloy J, McGloin D, (eds) (2010) Optical tweezers: methods and applications (Series in Optics and Optoelectronics). Thaylor and Francis Group
Parkin S, Knoner G, Nieminen T, Heckenberg N, Rubinsztein-Dunlop H (2006) Measurement of the total optical angular momentum transfer in optical tweezers. Opt Express 14:6963–6970
Perch-Nielsen I, Palima D, Dam J, Glückstad J (2009) Parallel particle identification and separation for active optical sorting. J Opt A: Pure Appl Opt 11:034013
Reicherter M, Haist T, Wagemann E, Tiziani H (1999) Optical particle trapping with computer-generated holograms written on a liquid-crystaldisplay. Opt Lett 24:608–610
Saleh B, Teich M (2008) Grundlagen der Photonik. Wiley-VCH, Berlin
Sasaki K, Koshioka M, Misawa H, Kitamura N, Masuhara H (1991) Pattern-formation and flow-control of fine particles by laser-scanning micromanipulation. Opt Lett 16:1463–1465
Shvedov V, Desyatnikov A, Rode A, Krolikowski W, Kivshar Y (2009) Optical guiding of absorbing nanoclusters in air. Opt Express 17:5743–5757
Shvedov V, Rode A, Izdebskaya Y, Desyatnikov A, Krolikowski W, Kivshar Y (2010) Giant optical manipulation. Phys Rev Lett 105:118103
Shvedov V, Rode A, Izdebskaya Y, Desyatnikov A, Krolikowski W, Kivshar Y (2010) Selective trapping of multiple particles by volume speckle field. Opt Express 18:3137–3142
Simmons R, Finer J, Chu S, Spudich J (1996) Quantitative measurements of force and displacement using an optical trap. Biophys J 70:1813–1822
Simpson N, Dholakia K, Allen L, Padgett M (1997) Mechanical equivalence of spin and orbital angular momentum of light: an optical spanner. Opt Lett 22:52–54
Stevenson D, Gunn-Moore F, Dholakia K (2010) Light forces the pace: optical manipulation for biophotonics. J Biomed Opt 15:041503
Stilgoe A, Nieminen T, Knoner G, Heckenberg N, Rubinsztein-Dunlop H (2008) The effect of Mie resonances on trapping in optical tweezers. Opt Express 16:15039–15051
Svoboda K, Block SM (1994) Biological applications of optical forces. Annu Rev Biophys Biomol Struct 23:247–285
Tolić-Nørrelykke S, Schäffer E, Howard J, Pavone F, Jülicher F, Flyvbjerg H (2006) Calibration of optical tweezers with positional detection in the back focal plane. Rev Sci Instrum 77:3101–3113
Viana N, Rocha M, Mesquita O, Mazolli A, Maia Neto P, Nussenzveig H (2007) Towards absolute calibration of optical tweezers. Phys Rev E: Stat Nonlinear Soft Matter Phys 75:021914
Visscher K, Brakenhoff G, Krol J (1993) Micromanipulation by "multiple" optical traps created by a single fast scanning trap integrated with the bilateral confocal scanning laser microscope. Cytometry 14:105–114
Volke-Sepulveda K, Garces-Chavez V, Chavez-Cerda S, Arlt J, Dholakia K (2002) Orbital angular momentum of a high-order Bessel light beam. J Opt B: Quantum Semiclass Opt 4:82–89
Wan J, Huang Y, Jhiang S, Menq C (2009) Real-time in situ calibration of an optically trapped probing system. Appl Opt 48:4832–4841
Woerdemann M, Alpmann C, Denz C (2012) Three-dimensional particle control by holographic optical tweezers. In: Osten W, Reingand N (eds) Optical Imaging and Metrology. Wiley-VCH Verlag, Weinheim, to be published

Zambrini R, Barnett S (2007) Angular momentum of multimode and polarization patterns. Opt Express 15:15214–15227

Zhang P, Zhang Z, Prakash J, Huang S, Hernandez D, Salazar M, Christodoulides D, Chen Z (2011) Trapping and transporting aerosols with a single optical bottle beam generated by moiré techniques. Opt Lett 36:1491–1493